Numerical study of sliding wear caused by a loaded pin on a rotating disc

Wenyi Yan, Noel P. O'Dowd*, Esteban P. Busso

Department of Mechanical Engineering, Imperial College of Science, Technology and Medicine, Exhibition Road, London SW7 2BX, UK

Abstract

A computational approach is proposed to predict the sliding wear caused by a loaded spherical pin contacting a rotating disc, a condition typical of the so-called pin-on-disc test widely used in tribological studies. The proposed framework relies on the understanding that, when the pin contacts and slides on the disc, a predominantly plane strain region exists at the centre of the disc wear track. The wear rate in this plane strain region can therefore be determined from a two dimensional idealisation of the contact problem, reducing the need for computationally expensive three dimensional contact analyses. Periodic unit cell techniques are used in conjunction with a ratchetting-based failure criterion to predict the wear rate in the central plane strain region. The overall three dimensional wear rate of the disc is then determined by scaling the plane strain wear rate with a conversion factor related to the predicted shape of the wear track. The approach is used to predict pin-on-disc test data from an Al–Si coating using a tungsten carbide pin. The predicted results are found to be consistent with measured data. © 2002 Elsevier Science Ltd. All rights reserved.

Keywords: A. Wear and ablation; B. Contact mechanics; B. Elastic–plastic material; C. Finite elements

1. Introduction

The sliding wear caused by a loaded spherical pin contacting a rotating disc is typical of that which occurs in pin-on-disc tests used to study friction and wear phenomena (see, e.g., Gee, 1993, ASTM and ASM, 1997). In a pin-on-disc test, see Fig. 1, the pin is held stationary under a specified load, while the disc rotates beneath it at a

---

* Corresponding author. Tel.: +44-020-7594-7059; fax: +44-020-7594-7017.
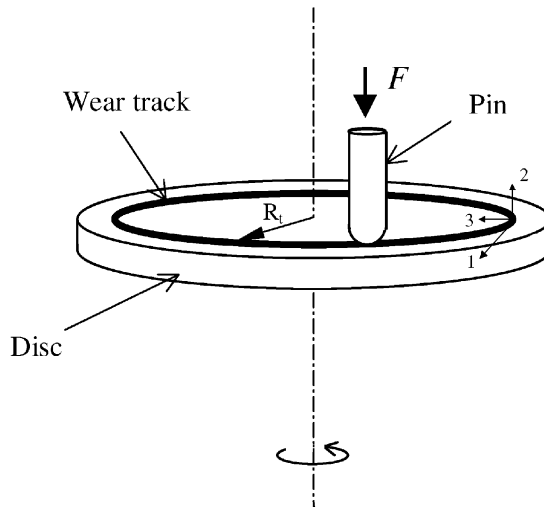 *E-mail address:* n.odowd@ic.ac.uk (N.P. O'Dowd).

Fig. 1. Schematic illustration of a pin-on-disc wear test.

constant velocity. If a sliding wear mechanism is being examined, the pin generally has a spherical head and the disc is fabricated from the material whose wear behaviour is investigated which is usually much softer than the pin material. The results obtained from a pin-on-disc test are usually expressed in the form of a wear rate, defined as the volume of material removed per sliding distance for a given load.

In view of its extensive use by the tribology community, it is surprising that little work has been carried out on the modelling of the pin-on-disc test. Poedra and Andersson (1999) examined the deformation of a disc contacted by a loaded pin using the finite element method. However, their work relied on an elastic axisymmetric model of static contact and the effects of plasticity and friction due to sliding contact were not considered. Stalin-Muller and Dang Van (1997) calculated the plastic strain field in the subsurface of a disc during a pin-on-disc test numerically by treating the contact problem as a steady state one, whereby the observer is assumed to be moving with the contact load. However, the wear rate was not predicted directly and no specific wear criterion was invoked.

More recently, Molinari et al. (2001) studied the wear caused by a pin sliding over a plate using finite element techniques. In their work, full three-dimensional (3D) elasto-plastic calculations were carried out to determine the stress and strain state in the contacting materials. The Archard wear law (Archard (1953)) was then used to determine the wear rate of the plate material. Although Archard's law was originally developed as a model for adhesive wear, it has been applied to a wide variety of wear conditions. However, it is phenomenological in nature and therefore provides little insight into the dominant wear mechanism. In addition, there is an inherent limitation associated with 3D non-linear sliding contact calculations in that they are extremely costly and time consuming, making parametric studies impracticable

and generally requiring unrealistic simplifications to the actual geometry of the problem. Thus, there is a strong need for a more computationally efficient mechanistic modelling approach to improve the understanding of wear in standard wear tests, such as the pin-on-disc test, and to aid in the development and validation of wear models. In this work, a mechanism-based continuum mechanics modelling approach is proposed to predict the sliding wear caused by a loaded pin sliding on a flat disc. The approach relies on an approximation of 3D wear rates by appropriately scaling wear rates obtained from 2D sliding contact finite element calculations. In this way, the required computational effort and solution times can be considerably reduced.

Under cyclic sliding contact, Kapoor and Johnson (1994) have proposed three regimes of wear. At low contact loads, the response can be either predominantly elastic or lead to an elastic shakedown, in which case the failure mechanism is similar to those observed in high cyclic fatigue. At higher loads, plastic shakedown will prevail when a constant uniaxial equivalent plastic strain amplitude is generated over each sliding cycle. This condition is analogous to that, seen in low cycle fatigue and thus similar failure mechanisms are expected. The third regime is associated with a continuous increase in the overall plastic strain, which accumulates in each sliding cycle, that is a ratchetting state develops (see also Rigney et al., 1992). Examination of a range of sliding contact experimental data (see e.g. Kapoor, 1994; discussion in Yan et al., 2000) has revealed that ratchetting is the predominant failure mode under conditions of cyclic sliding contact. Thus a ratchetting wear mechanism will be considered in this work.

In the computational model of sliding wear recently formulated by the authors (Yan et al., 2000), the contacting surfaces were idealised as having periodic roughness and the accumulation of plastic deformation in the subsurface was determined using unit cell and finite element (FE) techniques. In the current work, this framework is generalised to simulate the sliding wear caused by a loaded spherical pin on a rotating disc by treating the pin as a single asperity sliding continuously on the disc. Furthermore, the method of Yan et al. (2000), which dealt only with 2D wear states, is extended here to account for the 3D nature of sliding contact for a loaded spherical pin sliding on a disc. As the deformation of the central layer along the wear track is constrained laterally by the material away from the wear track, predominantly plane strain conditions may be assumed to prevail within this central region. Based on this assumption, a factor is introduced to convert the wear rate obtained from 2D plane strain calculations to the actual wear rate associated with the 3D sliding contact conditions typical of the contacting pin-on-disc problem. The conversion factor is estimated from the plastic deformation field in the subsurface of the disc obtained from a 3D FE analysis of a static (non-sliding) contact between the loaded pin and the disc.

The structure of the work presented below is as follows. The computational framework used to model the contacting pin and disc problem is first described in Section 2. The finite element simulation of the pin-on-disc problem is next discussed in Section 3, followed by a comparison between the model predictions and the measured data. Further discussion of the proposed methodology is provided in Section 4 and a summary is given in Section 5.
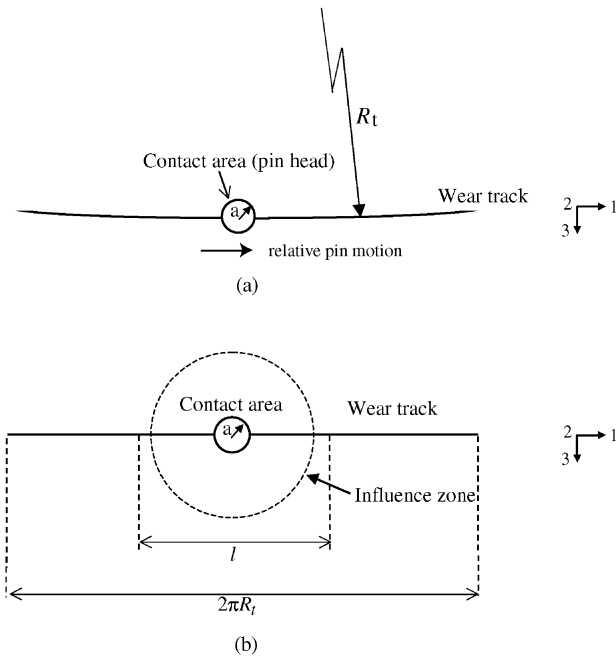
Fig. 2. Generalised pin-on-disc unit cell model: (a) view of a section of the wear track (see Fig. 1) including the contact area, and (b) generalised periodic unit cell of width l.

2. Computational framework

2.1. Three dimensional unit cell model

The relevant length scales of the contact problem associated with a loaded pin in contact with a rotating disc are the contact radius, a, and the wear track radius, R_t, as illustrated in Fig. 2(a). Generally, $a \ll R_t$ and the problem can therefore be treated as periodic with the pin considered to slide along a straight wear track, of length $2\pi R_t$, as illustrated in Fig. 2(b). The value of a depends on the compressive pin load, F, the pin head radius, and the material properties of the pin and disc, and may be estimated from contact (Hertz) theory (e.g. see Johnson, 1985) or obtained from finite element calculations.

For the contact problem shown in Fig. 2(b), the zone of influence of the pin is quite small—preliminary 3D FE analyses revealed the size of the highly deformed region generated by the contact between the pin and disc to be typically five times the contact area size, $2a$. The size of this influence zone is indicated in Fig. 2(b). Therefore, the problem can be further simplified by choosing the length of the unit cell, l, to be less than $2\pi R_t$ provided l is considerably greater than the size of the influence zone. An appropriate value for l will depend on the magnitude of the load, the pin dimensions and the material properties of the pin and disc. The choice of the length scale l will be discussed further in Section 4.
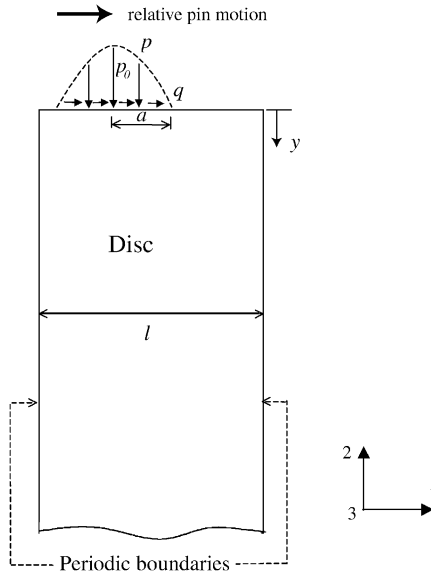
Fig. 3. Two-dimensional periodic unit cell model.

2.2. Two-dimensional wear formulation

A 2D periodic unit cell is illustrated in Fig. 3 (c.f. Yan et al., 2000). Wear is represented as the removal of a layer of material from the surface down to a depth b, which is the depth at which the plastic ratchetting strain reaches a maximum. Thus, the volume of material removed by sliding wear per unit thickness for a representative periodic unit cell of length l is

$$V = bl. \tag{1}$$

If the number of sliding cycles to failure is N_f, then the corresponding sliding distance, S, for each unit cell is

$$S = N_f l. \tag{2}$$

The 2D wear rate, W_{2D}, defined as the volume of material removed per unit thickness and sliding distance, is then

$$W_{2D} = \frac{V}{S} = \frac{b}{N_f}. \tag{3}$$

To determine the number of cycles to failure, the ratchetting-based wear model proposed in Yan et al. (2000) is invoked. The ratchetting strain at a given material point over a sliding cycle is defined as

$$\delta\varepsilon_{eff}^N = \varepsilon_{eff}^N - \varepsilon_{eff}^{N-1}, \tag{4}$$

where $N-1$ and N indicate successive sliding cycles, and ε_{eff} is an effective plastic strain measure,

$$\varepsilon_{\text{eff}} = \sqrt{\frac{2}{3}\varepsilon_{ij}^{\text{p}} \cdot \varepsilon_{ij}^{\text{p}}}. \tag{5}$$

Here, $\varepsilon_{ij}^{\text{p}}$ are the components of the current plastic strain tensor (they are the incrementally updated components of the plastic strain rate tensor to be defined in Section 3.1) and the sum is implied for $i,j = 1,3$. A similar effective plastic strain has been used in the study of fretting by Ambrico and Begley (2000). The accumulated ratchetting strain, $\bar{\varepsilon}_{\text{eff}}$, after N_{f} cycles at any point in the disc is given by

$$\bar{\varepsilon}_{\text{eff}} = \sum_{i=1}^{N_{\text{f}}} \delta\varepsilon_{\text{eff}}^{i}. \tag{6}$$

Failure due to ratchetting occurs once $\bar{\varepsilon}_{\text{eff}}$ exceeds the local ductility of the material, ε_{f}. Note that the material ductility, ε_{f}, typically depends on the local stress triaxiality. In Yan et al. (2000), the material ductility is assumed to be independent of triaxiality and thus failure is predicted to occur at the position(s) of maximum accumulated plastic strain. Due to the lack of experimental data required to quantify the effect of triaxiality on failure strain during cyclic sliding, the same assumption is made in this work. It should be noted that the triaxiality experienced by the coating in a pin-on-disc test is expected to differ considerably from that which would be obtained from e.g. a uniaxial tension test. However, since the conditions experienced in the pin-on-disc test are expected to match closely those experienced in service, the failure strain determined from the pin-on-disc test is expected to be also relevant for the prediction of the in-service life of the coating.

Under repeated sliding contact loading, Yan et al. (2000) found that after a sufficient number of sliding cycles the deformation reaches a steady state, i.e., the magnitude of the ratchetting strain no longer changes between cycles. Such a steady state may be reached after a relatively small number of cycles, much smaller than the number of cycles to failure, N_{f}. Thus the local failure condition at a point may be approximated as

$$\bar{\varepsilon}_{\text{eff}} = N_{\text{f}}\delta\varepsilon_{\text{eff}} \geqslant \varepsilon_{\text{f}}, \tag{7}$$

where $\delta\varepsilon_{\text{eff}}$ is the steady state effective ratchetting strain.

The number of cycles to failure can therefore be written as

$$N_{\text{f}} = \frac{\varepsilon_{\text{f}}}{\delta\varepsilon_{\text{eff}}}. \tag{8}$$

From Eqs. (3) and (8), the 2D wear rate is then given as

$$W_{\text{2D}} = \frac{\delta\varepsilon_{\text{eff}}b}{\varepsilon_{\text{f}}}. \tag{9}$$

In the 2D unit cell calculations, the pin is not modelled explicitly. Instead shear and normal tractions, consistent with the load applied on the disc by the pin, are applied on the unit cell surface, as shown in Fig. 3. It is assumed that the surface of the disc is perfectly smooth, i.e. the scale of the surface roughness is much smaller than the

contact radius, a. Note that, in principle, there is no difficulty in introducing periodic roughness on the disc surface. The normal traction applied on the surface of the disc, p, is extracted from a static (non-sliding) 3D elastic–plastic contact analysis of the pin and disc, which will be discussed in the next section. The distribution of the shear traction, q, is calculated using the Amontons–Coulomb friction law

$$q = \mu p, \tag{10}$$

where μ is the friction coefficient. Sliding contact is simulated by continuously moving the distributed tractions on the disc surface from left to right (i.e. along the positive x_1 direction in Fig. 3). One complete sliding cycle, corresponding to one full $360°$ rotation of the disc, is therefore simulated by moving the shear and normal tractions along the whole surface of the unit cell. Implicit in this approach is the assumption that the contact pressure does not change significantly during the cyclic contact between pin and disc due to, for example, changes in the surface profile of the pin or disc during the wear process.

2.3. 2D–3D scaling procedure

For 2D loading states, a uniform strip of disc material is assumed to be removed once the failure condition given by Eq. (7) is satisfied. However, the wear caused by the relative sliding between the pin and the disc is an inherently 3D problem, so the variation of plastic strain across the width of the contact region (see Fig. 2) must be considered. In principle, the procedure developed by the authors (Yan et al., 2000) can be applied directly to a 3D unit cell model and the wear rate obtained by simulating a 3D sliding contact process. However, the computational resources and solution times required to carry out full 3D sliding contact analyses are generally prohibitive. In this work, such limitation has been addressed by developing a procedure to scale appropriately the wear rate obtained from a 2D FE simulation to account for the three dimensional nature of the contact conditions in a contacting pin-on-disc problem.

A cross-section of the wear track is illustrated schematically in Fig. 4. The cross-section shown contains the axis of the pin and is normal to the direction of motion of the pin relative to the disc. The main assumption made to estimate the wear rate in the disc from 2D simulations is that plane strain conditions hold in a small region in the centre of the wear track (viz. region A_C in Fig. 4) due to the lateral constraint exerted by the disc material away from the wear track. (The existence of this plane strain region will be confirmed for the case of a loaded stationary pin in Section 3.) Two dimensional simulations therefore enable wear rate predictions (i.e. volume of material removed per unit sliding distance) in the region A_C.

The total volume of material removed per unit sliding distance, W_T, is defined as

$$W_T = \frac{A}{N_f}, \tag{11}$$

where A is the cross-sectional area of the wear track and N_f is the number of sliding cycles required to remove the material in the wear track. Similarly, the volume of material removed per unit sliding distance in the plane strain region of cross-sectional
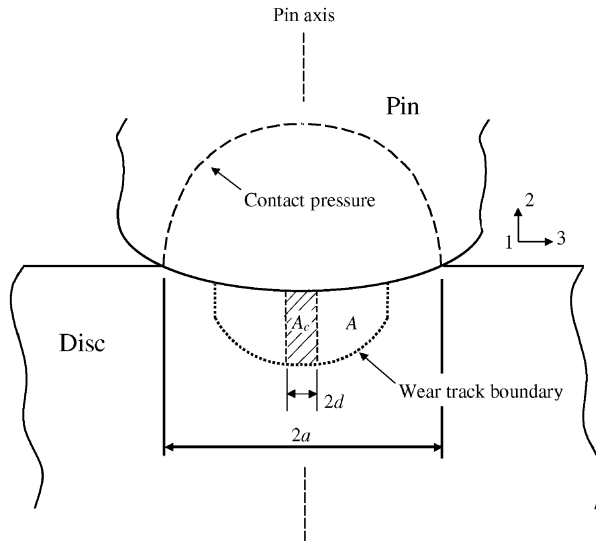
Fig. 4. Illustration of the wear track profile for a cross-section normal to the sliding direction and containing the axis of the pin.

area A_C is given by

$$W_C = \frac{A_C}{N_f}. \tag{12}$$

From Eqs. (11) and (12), the ratio between the overall wear rate and the wear rate in the central plane strain region is

$$\frac{W_T}{W_C} = \frac{A}{A_C}. \tag{13}$$

It should be noted that the wear rate obtained from a 2D FE analysis, W_{2D}, is the wear rate *per unit width* in the plane strain region of the wear track. Thus, the volume of material removed per unit sliding distance in the central plane strain region is

$$W_C = 2d W_{2D}, \tag{14}$$

where $2d$ is the width of the plane strain region of the wear track (see Fig. 4). Using Eqs. (13) and (14), the overall wear rate, W_T, can than be expressed in terms of W_{2D}, the width of the wear track, $2a$, and a conversion factor

$$\alpha = \frac{d}{a} \frac{A}{A_C}, \tag{15}$$

so that

$$W_T = \alpha \, 2a \, W_{2D}. \tag{16}$$

Thus, to obtain the overall wear rate from the 2D wear rate, the quantities A, A_C and d are required. These quantities, which are related to the shape of the wear track profile, are not known a priori and must be estimated. It may be noted that if predominantly

plane strain conditions prevail in the wear track region, then $A_C \approx A$, $d \approx a$ and Eq. (15) yields $\alpha \approx 1$. Thus a value of α less than unity will indicate a deviation from a predominantly plane strain state.

As discussed earlier, failure is assumed to occur when the accumulated ratchetting strain ($\bar{\varepsilon}_{eff}$) exhausts the local material ductility. Therefore, the wear track boundary, i.e. the boundary which encloses the region A in Fig. 3, should correspond to a locus of material points where $\bar{\varepsilon}_{eff} \geqslant \varepsilon_f$. Furthermore, the width of the central plane strain region $2d$ is given by the extent of the region where plane strain conditions hold, that is where $\bar{\varepsilon}_{eff}$ is independent of the coordinate x_3 (see Fig. 4). In principle, such information can be obtained from full 3D sliding contact simulations, involving large computing resources, and, in effect, negating the need for the 2D–3D conversion procedure discussed in this section. In this work, 3D static (i.e. non-sliding) contact simulations are carried out to obtain an estimate of α in Eq. (16). The wear track profile is estimated by the contours of effective plastic strain, ε_{eff}, in the cross-section containing the axis of the pin and normal to the sliding direction at a given pin load. It is expected that the contour shapes obtained from these analyses will not differ significantly from those which prevail under ratchetting conditions.

The value of the conversion factor α in Eq. (16) cannot be determined uniquely as it will depend on the particular level of effective plastic strain chosen to define the wear track. Thus, the boundary of the wear track profile of cross-sectional area A is defined by the region enclosed by the locus of material points where

$$\varepsilon_{eff} = \beta \varepsilon_{eff}^{max}. \tag{17}$$

Here, β is a parameter which varies between 0 and 1 and ε_{eff}^{max} is the maximum effective plastic strain computed from a 3D static contact analysis for a given pin load. Under predominantly plane strain conditions, which would correspond to an infinitely wide wear track and which could be realised by an infinitely long cylindrical pin sliding on a flat plate, $\beta = 1$ since the maximum plastic strain does not vary across the wear track. In a 3D analysis, β must chosen to be less than or equal to 1 in order to obtain a finite sized wear track. Specific examples of the choice of β and its effect on the conversion factor α will be discussed in Section 3.

The full procedure for the determination of the wear rate in the contacting pin and disc problem is illustrated by the flow chart of Fig. 5. Note that the 3D contact simulation provides the pressure distribution to be used in the 2D unit cell calculations as well as the wear track shape characteristics to determine the 2D–3D conversion factor α. Next we discuss a case study illustrating the procedure.

3. Analysis of the pin-on-disc test

3.1. Material properties

The wear behaviour of a 200 μm Al–Si coating deposited on a carbonised steel substrate and subjected to cyclic sliding contact with a tungsten carbide pin is investigated in this section.
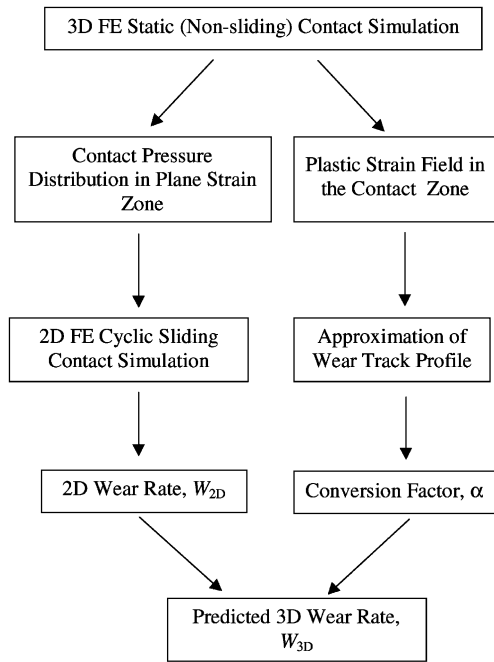
Fig. 5. Procedure to obtain 3D wear rates.

The coating material properties were determined from microindentation data using a method recently developed by Tunvisut et al. (2001). The mean value of the yield stress for the Al–Si coating, σ_{yc}, was found to be 640 MPa, and the Young's modulus, 71 GPa. For the wear analysis, it is necessary to specify the cyclic stress–strain response of the coating material. Here, the coating is assumed to be a Von Mises rate-independent elasto-plastic material which hardens kinematically. During active yielding, the plastic deformation rate tensor, $\dot{\boldsymbol{\varepsilon}}^{p}$, is given by,

$$\dot{\boldsymbol{\varepsilon}}^{p} = \frac{3}{2}\,\dot{\tilde{\varepsilon}}^{p}\,\frac{\boldsymbol{T'} - \boldsymbol{B}}{\tilde{\sigma}}, \tag{18}$$

where $\dot{\tilde{\varepsilon}}^{p}$ is the magnitude of the Mises equivalent plastic strain rate and $\tilde{\sigma}$ is the equivalent stress,

$$\tilde{\sigma} = \sqrt{\tfrac{3}{2}(\boldsymbol{T'} - \boldsymbol{B}):(\boldsymbol{T'} - \boldsymbol{B})}, \tag{19}$$

with $\boldsymbol{T'}$ the deviatoric component of the Kirchhoff stress, $\boldsymbol{T}, \boldsymbol{B}$ a kinematic hardening variable (often called the back stress). The evolution of $\boldsymbol{B}$ follows a hardening-dynamic recovery form (Ziegler, 1959),

$$\dot{\boldsymbol{B}} = (H\boldsymbol{T} - K\boldsymbol{B})\dot{\tilde{\varepsilon}}^{p}, \tag{20}$$

where H and K are dimensionless material constants and may be calibrated from cyclic stress–strain data. For the coating, $H = 2.48$ and $K = 5.43$ which are typical values for
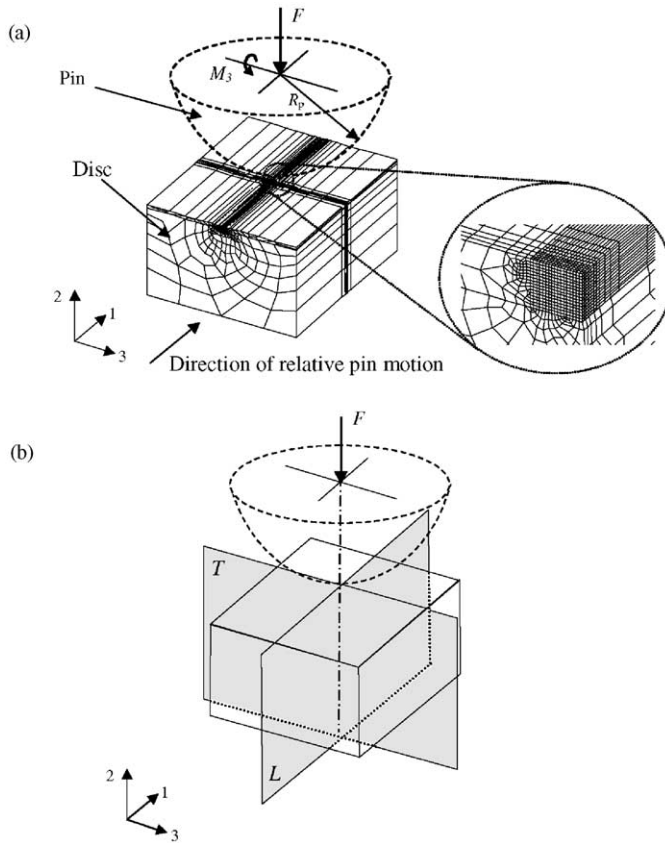
Fig. 6. (a) Finite element model used in the 3D static (non-sliding) contact analysis, (b) identification of transverse (T) and longitudinal (L) planes in the contact region.

ductile materials (Yan et al., 2000). The steel substrate, which exhibits little plastic deformation, has a yield strength of 2500 MPa and is assumed to be perfectly plastic (non-hardening).

In the static (non-sliding) contact analysis, the pin, which has a 3 mm radius and a yield strength of ≈ 5000 MPa, is treated as a rigid body as it is much harder than the coating.

3.2. Static (non-sliding) contact analysis

A 3D static (non-sliding) contact analysis is first required to determine the wear conversion factor, α, and the contact pressure distribution to be used in the 2D sliding contact simulations. The finite element model for the 3D static contact calculations is shown in Fig. 6(a)—in this case the FE mesh consists of approximately 18000 linear isoparametric 3D solid elements. A very fine mesh is employed in the contact zone
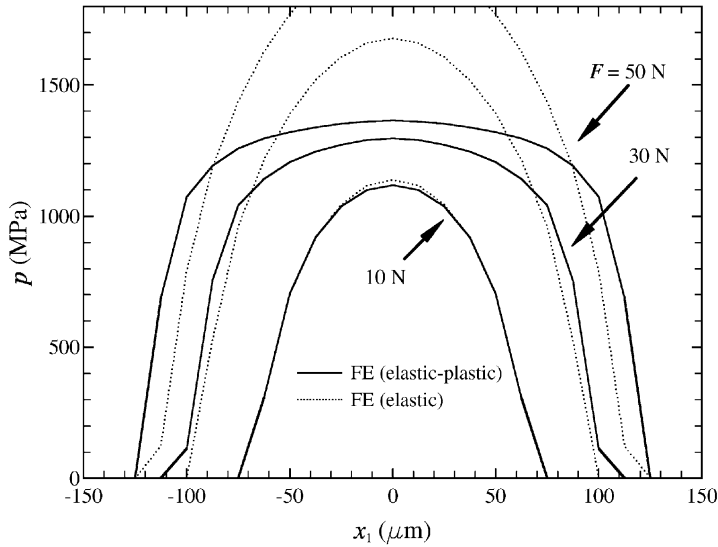
Fig. 7. Contact pressure distributions under different pin loads.

of the disc where the deformation gradients are the highest, as shown in the insert to Fig. 6(a). Note that, to carry out a 3D wear simulation directly, this fine mesh region would have to extend the full length of the unit cell to obtain an accurate solution. The normal load is applied through the axis of the rigid pin head of radius R_p and the friction force exerted on the disc due to sliding is realised by applying a moment to the pin about the x_3 axis (see Fig. 6), defined as

$$M_3 \approx \mu F R_p, \tag{21}$$

which implies that the pin is at the point of sliding on the disc. Thus, the shear force in the static analysis acts along the direction of motion of the pin relative to the disc in the actual sliding contact problem, i.e. along the x_1 direction in Fig. 6. This boundary value problem was solved using a commercial finite element program (ABAQUS, 1998). It should be noted that in the analysis, no advantage has been taken of the symmetry about the longitudinal plane (plane L in Fig. 6(b)) as the facility to specify a symmetry plane for the rigid surface used in the analysis was not available in the current version of the FE code.

The computed finite element contact pressure distributions in the central cross-section of the disc ($x_3 = 0$) along the x_1 direction are shown in Fig. 7 for three different pin loads, namely $F = 10, 30$ and 50 N. For comparison, the solutions from an elastic FE analysis of the static 3D contact problem also shown. It can be seen that, at the lowest load, the difference between the elastic and elastic–plastic distributions is small but the discrepancy increases with increasing load.

3.2.1. Strain state at the centre of the contact region

In order to justify the use of the conversion factor, α, Eq. (15), it is necessary to verify that the disc material experiences predominantly plane strain conditions in the central region of the wear track. For this to be the case, the shear strain components ε_{23} and ε_{13}, and the normal strain component ε_{33} must be equal or close to zero in the central region. In the results to be presented next, the magnitudes of these strain components relative to the norm of the strain tensor, namely

$$\varepsilon_a = \sqrt{\varepsilon_{ij}\varepsilon_{ij}} \tag{22}$$

will be examined. The FE results from the 3D static contact calculations for a pin load of 40 N are shown in Fig. 8. Here, distances are expressed in terms of the contact radius a, obtained from the finite element calculations.

Fig. 8(a) shows contours of the normalised shear strain component $|\varepsilon_{23}/\varepsilon_a|$ in a region of the transverse plane of the disc (plane T in Fig. 6(b)), of width $1.6a$ and height a. As indicated in Fig. 8(a), due to the symmetry of the loading, the deformation in this transverse plane is symmetric with respect to the pin axis. Thus, by definition, the shear strain components ε_{23} and ε_{13} must be zero in this plane. The FE results show that the magnitude of the shear strain component $|\varepsilon_{23}/\varepsilon_a|$ in a narrow region neighbouring the symmetry plane is less than 8%. Though not shown, ε_{13} is also negligibly small in the whole of the studied region. In Fig. 8(b), contour plots of the normal strain component $|\varepsilon_{33}/\varepsilon_a|$ in the same region are shown. It can be seen that the value of the normal strain ratio is low in the region just beneath the contact surface (except for a small region close to the contacting pin) and increases gradually with depth—its value is about $|\varepsilon_{33}/\varepsilon_a| = 0.29$ at $x_2 = -a$. Finally, Fig. 8(c) shows the variation of $|\varepsilon_{33}/\varepsilon_a|$ in the wear track symmetry plane, parallel to the sliding direction (plane L in Fig. 6(b)). It may be seen that the normal strain component remains close to zero within this plane for distances less than $\sim 0.5\,a$, apart from a small region very close to the surface.

Based on these results, it is clear that a plane strain region exists up to a depth of $\sim 0.5\,a$ below the contacting pin. For the proposed methodology to be valid, the maximum depth of the wear track must lie within this region. It will be shown in Section 3.3 that this condition holds for the pin-on-disc loading examined in this work.

3.2.2. Determination of the conversion factor α

The approximated wear track profiles obtained from the static contact analysis with a pin load of 40 N are shown in Fig. 9. The curved segments of these predicted wear track profiles correspond to contours of constant effective plastic strain defined by $\varepsilon_{\text{eff}} = \beta \varepsilon_{\text{eff}}^{\text{max}}$. The material points between these curved lines and the coating surface are assumed to be removed by wear leading to the straight line portion of the wear track profile seen in Fig. 9. The three wear profiles shown in Fig. 9 correspond to different values of β—the larger the value of β, the smaller the size of the predicted wear track. By comparing Figs. 9(a)–(c), it can be seen that the width of the plane strain region
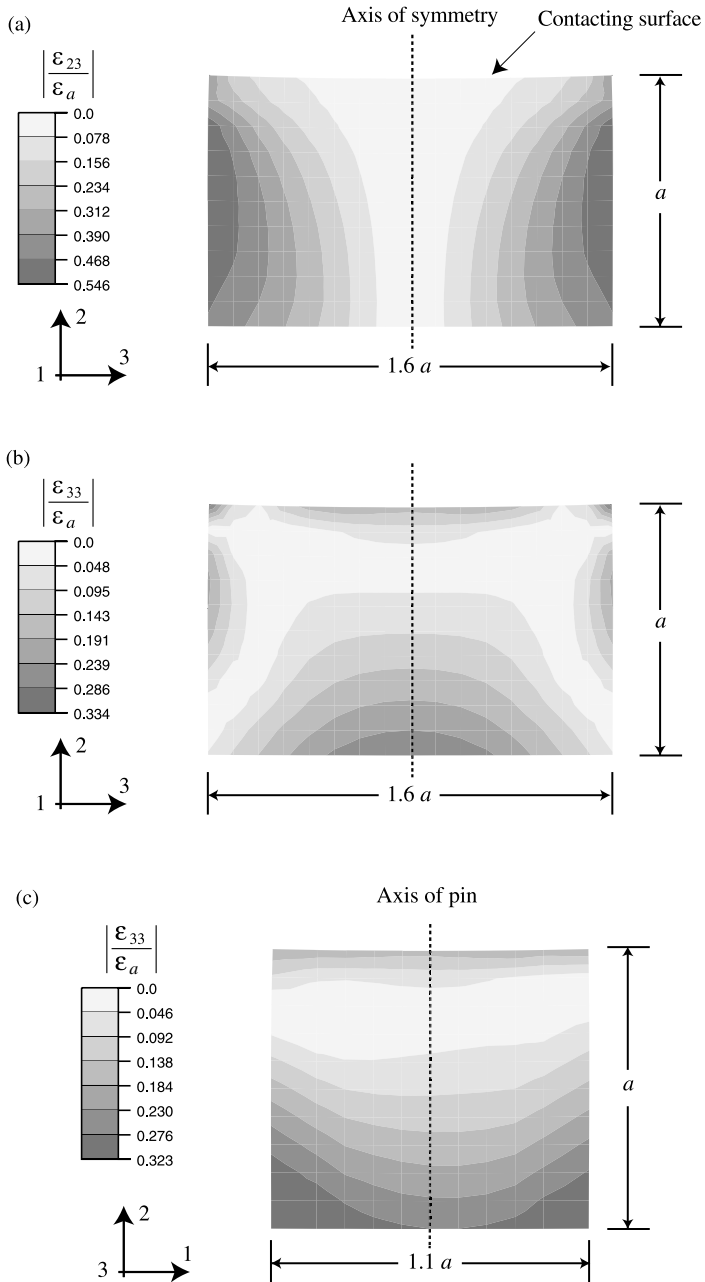
Fig. 8. Contours of the out-of-plane strain ratios in the sub-surface of the disc induced by static contact with the pin (a) $|\varepsilon_{23}/\varepsilon_a|$ in the transverse plane, (see Fig. 6(b)), (b) $|\varepsilon_{33}/\varepsilon_a|$ in the transverse plane, and (c) $|\varepsilon_{33}/\varepsilon_a|$ in the longitudinal plane. (Here ε_a is the norm of the strain tensor defined via Eq. (22).)
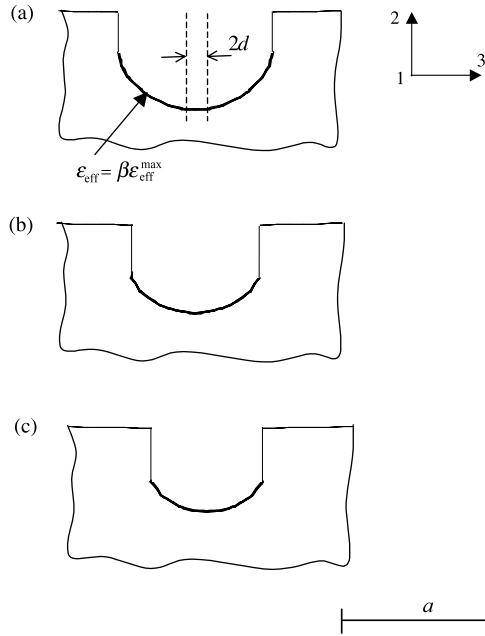
Fig. 9. Predicted wear track profiles for different values of the parameter β, (Eq. (17)) (a) $\beta = 0.75$, (b) $\beta = 0.85$, and (c) $\beta = 0.90$. The figures are plotted to the same scale, indicated above in terms of the corresponding contact radius a.

where the $\varepsilon_{\mathrm{eff}}$ line remains approximately parallel to the surface, given by the width $2d$ in Fig. 9(a), shows only a weak dependency on β.

The range of β values considered here leads, via Eq. (15), to a corresponding range of values for the conversion factor α. This will, in turn, result in a range of predicted overall wear rates through Eq. (16). The dependence of α on β for four different pin loads is illustrated in Fig. 10. It can be seen that the calibrated conversion factor α varies by approximately 30% over the range $0.75 \leqslant \beta \leqslant 0.9$. As shown in Fig. 9(c), a high value of β results in a narrow wear track and a small value for α. On the other hand, Fig. 10 shows that, for a given β, α increases with normal load, F. This is due to the fact that, as seen in Fig. 7, the contact pressure distribution in the central region of the wear track is almost constant within a wide region at high pin loads. In such cases, the plane strain zone is therefore wider leading to a higher value of α. (It should be recalled that, in the plane strain limit, $\alpha = 1$.)

3.3. Determination of the wear rate

The pressure distributions calculated from the 3D static elastic–plastic contact simulations, e.g. see Fig. 7, are here applied in a 2D unit cell analysis as described in Section 2.2.
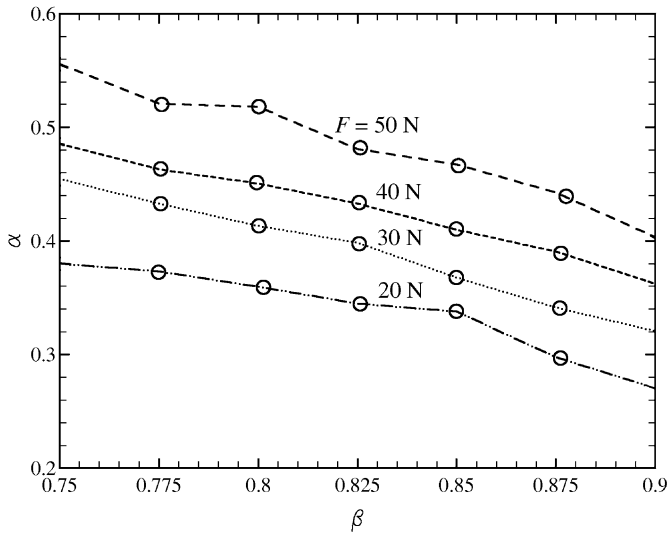
Fig. 10. Influence of the parameter β (Eq. (17)) on the 2D–3D conversion factor α (Eq. (15)) for different load levels with $\mu = 0.11$.

The FE calculations reveal that, when the pin load is less than 7.75 N, no plastic strains are generated in the coating or substrate, and plastic ratchetting occurs in the coating for loads greater than 8 N. In this section, all the cases to be discussed correspond to the latter condition. The test was carried out with lubrication, resulting in a measured friction coefficient of 0.11 (COMPWERC, 1998). Therefore the temperature increase in the disc due to friction is expected to be small and the mechanical properties evaluated at room temperature (yield strength and hardening properties) are expected to remain valid for the simulation of the wear test.

Fig. 11 illustrates the shear stress, σ_{12}, normalised by the yield strength of the coating, σ_{yc}, plotted against shear strain, ε_{12}, normalised by the coating yield strain, ε_{yc}, at a material point in the coating. Fig. 11(a) illustrates the initial stages of the cyclic deformation and Fig. 11(b) the cyclic response in the steady state regime. It may be seen that the cyclic variation of shear stress is not symmetric about zero, i.e. there is a non-zero mean stress. Furthermore, although the amplitude of the shear stress remains constant from cycle to cycle, the plastic shear strain increases continuously.

The predicted variation of the effective plastic strain, ε_{eff}, in the coating subsurface at different sliding cycles is shown in Fig. 12(a) for $F = 40$ N. Here y measures depth below the contacting surface (see Fig. 3). It is seen that the maximum value of ε_{eff} always occurs at approximately the same distance from the contacting surface, here denoted by the depth b. Note that $b \approx 0.3a$ indicating that the peak ratchetting strain occurs within the plane strain region identified in Section 3.2.1 (see also Fig. 8). The increase in the effective strain per cycle, $\delta\varepsilon_{eff}^{N}$, defined via Eq. (5), at this depth as the number of sliding cycles increases is shown in Fig. 12(b). It can be seen that after
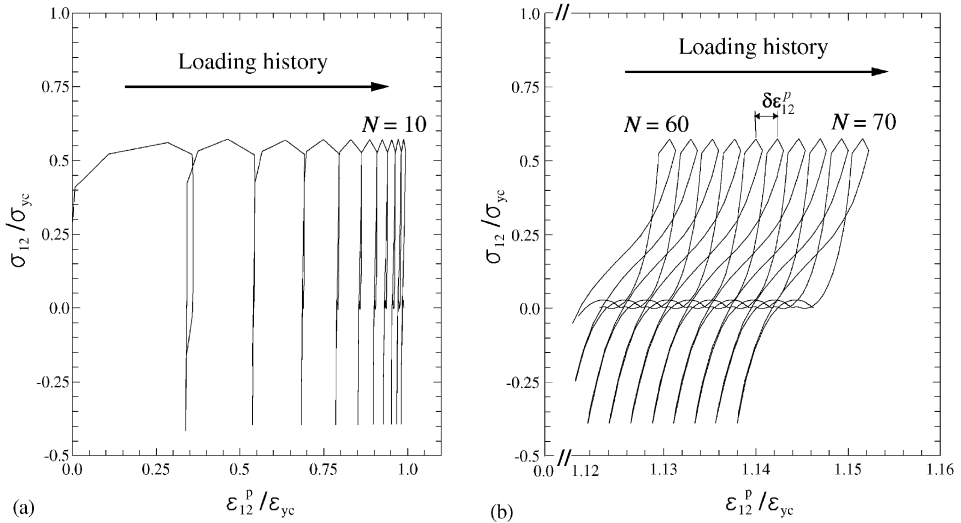
Fig. 11. Illustration of the ratchetting behaviour of the plastic shear strain component, $\varepsilon_{12}^{\mathrm{p}}$, in the disc during cyclic sliding: (a) initial evolution, and (b) steady state regime.

approximately 20 cycles a constant ratchetting strain is obtained. It is this steady state value which is used to estimate the number of sliding cycles to failure.

In the 2D numerical analysis, approximately 1000 equilibrium iterations are required for each sliding cycle (i.e. to move the load across the unit cell). As seen in Fig. 12(b), about 20 cycles are needed to reach steady state. (To ensure that steady state conditions were achieved, the analyses presented here were run for 100 sliding cycles.) Thus, approximately 20 000 matrix inversions are required in an implicit analysis to obtain the steady state ratchetting strain required to determine the wear rate. Some trial calculations are required to determine the unit cell length l, the minimum length at which the analysis becomes independent of l. For the load range of interest, after a number of trial calculations, solutions independent of l were found for $l \geqslant 1.25$ mm, which is over five times the maximum contact area size, $2a$.

Fig. 13 shows the predicted increase in normalised 2D wear rate with applied load. The predicted overall wear rate W_{T} for the pin-on-disc test can be estimated from Eq. (16) and the results of Fig. 13. These predictions are shown in Fig. 14. For a given load, a range of wear rates is predicted depending on the choice of β. The measured data from the pin-on-disc tests are also shown in Fig. 14 (see COMPWERC, 1998). Choosing the material ductility for the Al–Si coating, ε_{f}, as 0.5, the measured data are consistent with the predictions.

4. Discussion

A computational framework has been proposed to predict the wear rate caused by a spherical pin sliding on a flat disc. A number of approximations and simplifications
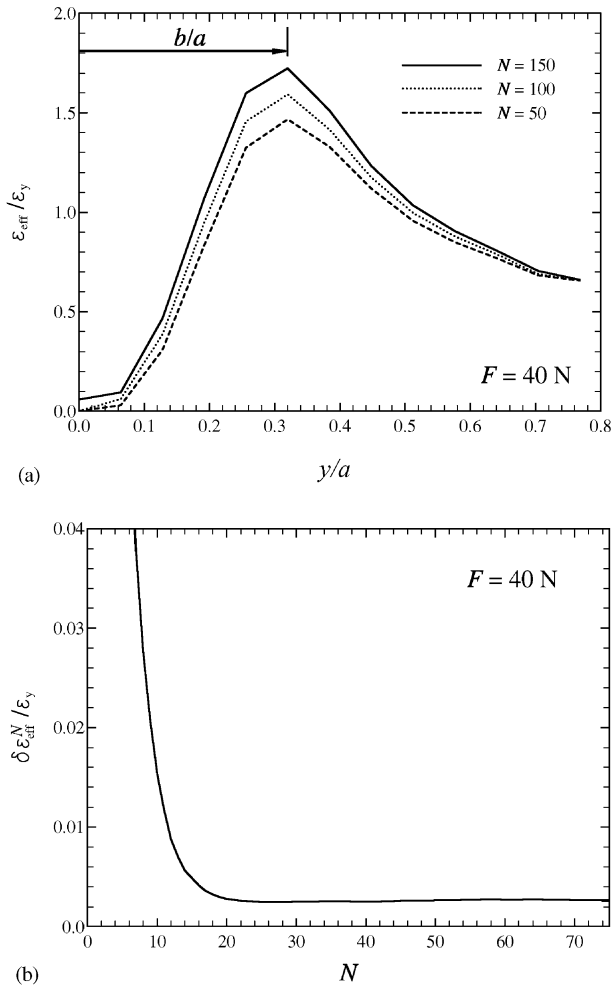
Fig. 12. (a) Variation of the normalised effective plastic strain as a function of normalised distance from the contact surface at different sliding cycles, and (b) variation of the effective ratchetting strain $\delta\varepsilon_{\text{eff}}^N$ at depth b with sliding cycle N. Note that after ≈ 20 sliding cycles, $\delta\varepsilon_{\text{eff}}^N$ reaches a steady state.

have been made to allow the problem to be modelled efficiently while still retaining its most important features. Some further issues related to the use of the approach in predicting actual wear behaviour are discussed below.

The 2D wear rate from Eq. (9) is determined by considering the removal of a layer of material of depth b. After this layer is worn away, the pin will then be in contact with a new material surface. If sliding contact continues, it is expected that this material will experience a similar accumulation of plastic deformation as the first, and a second layer of material of approximately the same thickness will then be removed due to ratchetting. The number of sliding cycles to failure for the second layer will
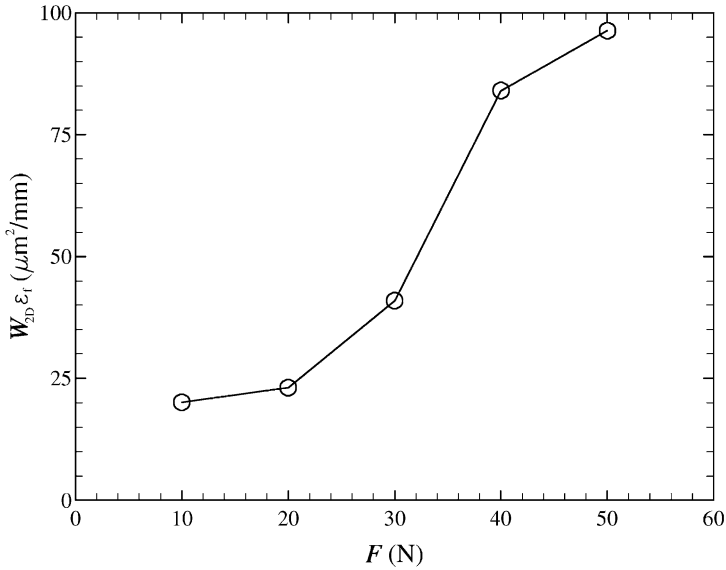
Fig. 13. Predicted normalised 2D wear rate of the Al–Si coating as a function of pin load.
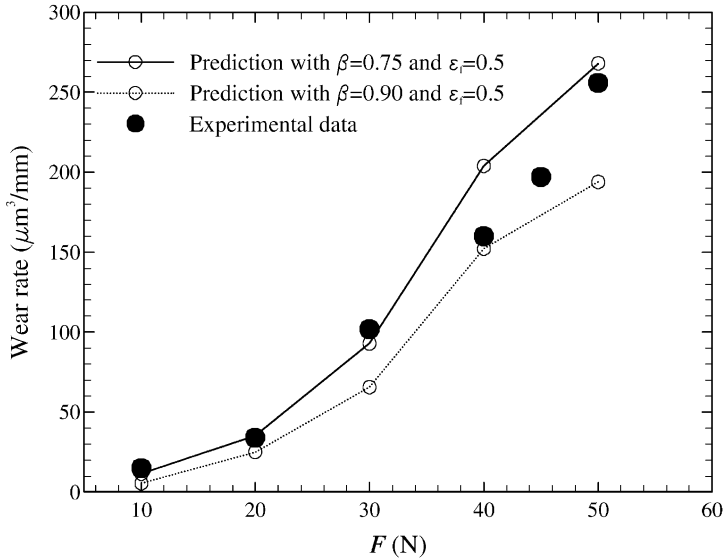

Fig. 14. Predicted and measured wear rate of an Al–Si coating in a pin-on-disc test as a function of pin load.

be smaller than that of the first layer as a certain amount of plastic deformation will accumulate in the second layer as the first layer is being worn away. Thus, the wear rate for the second layer should be higher than that for the first and so on for subsequent layers until the test is completed. The wear rate for the first layer is therefore expected

to be lower than the average wear rate for the whole process. However, due to the steep nature of the local strain gradients at the critical depth b, e.g. see Fig. 12, the number of sliding cycles to failure of each layer is expected to depend weakly on the strain accumulated during the failure of preceding layers. Therefore the predicted wear rate should not differ significantly from what would be obtained if the complete wear process (i.e. removal of successive layers of material) during the pin-on-disc test were modelled. It should also be noted that any effect of the changing geometry of the problem has been ignored here—the wear track will become deeper and wider as material is gradually removed, which may lead to a change in the size of the plane strain zone. This issue has not been examined here.

The results presented in Fig. 14 show good agreement between the measured and predicted wear rates for the Al–Si coating. This agreement was achieved by taking the material ductility, ε_f to be 0.5. For the case of cyclic sliding contact, Kapoor and Franklin (2000) suggest that material ductility should range from about 2.5–10. If the value for ε_f was chosen to lie within this range, the predicted wear rates would be considerably lower than the measured ones. In reality, the coating deposition process generally introduces inhomogenieties in the material, such as inclusions, porosities and oxides. The wear behaviour of inhomogeneous coatings has been examined in Yan et al. (2001) where it was found that the wear rate is considerably enhanced when inhomogeneities, such as micro-voids, are introduced into the material, due to the local amplification of the strain in the vicinity of the homogeneities. The value of the failure strain inferred from this analysis, implicity accounts for the presence of such inhomogeneities and is therefore lower than the value which would be obtained for a fully dense coating. Provided the same coating deposition conditions which prevailed during coating of the disc used in the pin-on-disc test also hold during coating of an actual component, the failure strain determined from a pin-on-disc test using the methods illustrated here will also be representative of the failure strain of the in-service coating.

In Section 3, the profile of the wear track has been approximated by examining contours of constant effective plastic strain. It has been found that the measured wear tracks, (see COMPWERC, 1998) are somewhat different from the predicted ones—the measured profiles tending to have a much lower aspect ratio (i.e. they are shallower and wider) than those predicted by the analysis. There are at least two possible explanations for such discrepancy:

Firstly, it is difficult to ensure that the pin describes a perfect and repeatable circle during each sliding cycle in the test. The resultant variations in the relative distance between the axes of the pin and disc would lead to a wider wear track. The measured width of the wear track in the Al–Si pin-on-disc test was typically about 430 μm at a pin load of 40 N. This is considerably larger than the corresponding calculated contact area ($2a = 250$ μm) suggesting that the pin could not have inscribed a perfect circle throughout the test. If the pin departs systematically from the original wear track, then the number of sliding cycles experienced by a given material point will be less than the number of disc rotations (in this work it is assumed that the number of sliding cycles is equal to the number of disc rotations). This effect, which

is expected to be independent of load, will result in an overestimate of the failure strain, ε_f, by the model, but does not invalidate the approach used.

Secondly, wear debris may not be removed along paths of constant effective plastic strain as assumed in the model. The profile of the wear track may, in addition depend on local microstructural inhomogeneities and/or the local stress distributions (e.g. tri-axiality effects). The latter will be relevant in materials where local failure may be controlled by cleavage-induced microcracking. Further work, including a more detailed examination of experimental wear tracks, is being carried out in order to investigate these issues.

5. Summary

A computational mechanics-based approach has been proposed to predict the sliding wear caused by a loaded spherical pin contacting a rotating disc. The central region of the wear track has been considered to experience plane strain conditions and a recently developed ratchetting wear model has been applied to estimate the rate of wear caused by the relative sliding between the pin and the disc. An important aspect of the proposed approach is that it relies on the 3D plastic deformation field in the disc subsurface beneath a non-sliding contacting pin to infer the shape of the wear track and predict the overall wear rate. The proposed approach has been used to predict wear rates obtained experimentally in pin-on-disc tests on an Al–Si coating using a WC pin, and the predicted trend was found to be consistent with the experimental data.

Acknowledgements

References

ABAQUS, V.5.8, 1998. Hibbitt, Karlsson and Sorensen Inc., Providence, RI.

Ambrico, J.M., Begley, R., 2000. Plasticity in fretting contact. Journal of Mechanical Physics Solids 48, 2391–2417.

Archard, J.F., 1953. Contact and rubbing of flat surfaces. Journal of Applied Physics 24, 18–28.

ASTM, ASM, 1997. Friction and wear testing source book of selected references from ASTM standards and ASM handbooks/ASTM, Materials Information Society, West Conshohocken, PA: ASTM; Materials Park, OH.

COMPWERC, 1998. Computational modelling of wear resistant coatings. Brite EuRam project, BE97-4283.

Gee, M.G., 1993. Guidelines for unlubricated sliding wear tests. DMM(A)96-97. National Physical Laboratory, UK.

Johnson, K.L., 1985. Contact Mechanics. Cambridge University Press, Cambridge.

Kapoor, A., 1994. A re-evaluation of the life to rupture of ductile metals by cyclic plastic strain. Fatigue Fract. Engng Mater. Struct. 17, 201–219.

Kapoor, A., Franklin, F.J., 2000. Tribological layers and the wear of ductile materials. Wear 245, 204–215.

Kapoor, A., Johnson, K.L., 1994. Plastic ratchetting as a mechanism of metallic wear. Proceedings of the Royal Society of London A 445, 367–381.

Molinari, J.-F., Ortiz, M., Radovitzky, R., Repetto, E.A., 2001. Finite element modeling of dry sliding wear in metals, Eng. Comp. submitted.

Poedra, P., Andersson, S., 1999. Simulating sliding wear with finite element method. Tribology International 32, 71–81.

Rigney, D.A., Divakar, R., Kuo, S.M., 1992. Deformation substructures associated with very large plastic strains. Scripta Met. Et. Mat. 27, 975–980.

Stalin-Muller, N., Dang Van, K., 1997. Numerical simulation of the sliding wear test in relation to material properties. Wear 203–204, 180–186.

Tunvisut, K., O'Dowd, N.P., Busso, E.P., 2001. Use of scaling functions to determine mechanical properties of thin coatings from microindentation tests. International Journal of Solids and Structures 38, 335–351.

Yan, W., Busso, E.P., O'Dowd, N.P., 2000. A micromechanics investigation of sliding wear in coated components. Proceedings of the Royal Society of London A 456, 2387–2407.

Yan, W., Busso, E.P., O'Dowd, N.P., 2001. A generalised sliding wear model for inhomogenous coatings, J de Physique IV in press.

Ziegler, H., 1959. A modification of Prager's hardening rule. Quarterly Applied Mathematics 17, 55–65.